

Multicontinuum Modeling of Time-Fractional Diffusion-Wave Equation in Heterogeneous Media

Huiran Bai^a, Dmitry Ammosov^b, Yin Yang ^{*a}, Wei Xie^a, and Mohammed Al Kobaisi^b

^aSchool of Mathematics and Computational Science, Xiangtan University, National Center for Applied Mathematics in Hunan, Xiangtan 411105, Hunan, China

^bChemical and Petroleum Engineering Department, Khalifa University of Science and Technology, Abu Dhabi, 127788, UAE

Abstract

This paper considers a time-fractional diffusion-wave equation with a high-contrast heterogeneous diffusion coefficient. A numerical solution to this problem can present great computational challenges due to its multiscale nature. Therefore, in this paper, we derive a multicontinuum time-fractional diffusion-wave model using the multicontinuum homogenization method. For this purpose, we formulate constraint cell problems considering various homogenized effects. These cell problems are implemented in oversampled regions to avoid boundary effects. By solving the cell problems, we obtain multicontinuum expansions of fine-scale solutions. Then, using these multicontinuum expansions and supposing the smoothness of the macroscopic variables, we rigorously derive the corresponding multicontinuum model. Finally, we present numerical results for two-dimensional model problems with different time-fractional derivatives to verify the accuracy of our proposed approach.

Keywords: multicontinuum, homogenization, time-fractional diffusion-wave equation, heterogeneous, multiscale, macroscopic.

1 Introduction

Many chemical and physical processes involve memory and genetic effects. It is known that fractional differential equations are better suited to modeling such processes than integer differential equations [1, 2]. Time-fractional diffusion-wave equations are generalizations of classical parabolic ($\alpha = 1$) and hyperbolic equations ($\alpha = 2$), which are derived by replacing the first- or second-order time derivative with a fractional derivative of order α with $0 < \alpha < 2$ [3]. In the case $0 < \alpha < 1$, we have the time-fractional diffusion or subdiffusion equation, while in the case $1 < \alpha < 2$, we obtain the superdiffusion equation, or the time-fractional wave equation, or the time-fractional diffusion-wave equation. The time-fractional diffusion-wave equation describes important physical phenomena that occur in amorphous, colloid, glass and porous materials, fractal and percolation clusters, comb structures, dielectric and semiconductor, biological systems, polymers, random and disordered media, geophysical and geological processes and the universal electromagnetic, acoustic, and mechanical processes (see [4, 5, 6, 7, 8, 9]).

In the past two decades, there have been many works dedicated to the time-fractional diffusion-wave equation (TFDWE). Mainardi and Paradisi [10] applied TFDWE to study the propagation of stress waves

*Corresponding author

E-mail addresses: 202331510101@smail.xtu.edu.cn (Huiran Bai), dmitrii.ammosov@ku.ac.ae (Dmitry Ammosov), yangyinxu@xtu.edu.cn (Yin Yang), xiew@smail.xtu.edu.cn (Wei Xie), mohammed.alkobaisi@ku.ac.ae (Mohammed Al Kobaisi).

in viscoelastic media relevant to acoustics and seismology. Sun and Wu [11] proposed a fully discrete difference scheme for TFDWE by introducing two new variables to transform the original equation into a low-order system of equations. Du et al. [12] proposed a compact difference scheme for the fractional diffusion-wave equation. Zhang et al. [13] presented the alternating direction implicit (ADI) method in the time stepping and a difference scheme combining the compact difference approach for spatial discretization for solving the two-dimensional TFDWE. Li and Li [14] presented a fast element-free Galerkin (EFG) method. Alikhanov [15] presented the investigation of a TFDWE involving a Caputo derivative and examined a more generalized model incorporating a memory kernel and the generalized Riemann–Liouville fractional integral.

However, many real problems have high contrast properties and complex heterogeneities at multiple scales. Examples include composite materials, porous media [16], turbulent transport in high Reynolds number flows [17], and others. Adopting traditional numerical methods for such multiscale problems is challenging even using supercomputers. Simulations of these problems are costly and can cause difficulties due to a large number of degrees of freedom. To reduce the computational cost, various upscaling techniques are often used to perform simulations on coarse computational grids.

Many different upscaling approaches have been exploited to solve multiscale problems on a coarse computational grid. Among these approaches, one can mention homogenization methods [18, 19]. The main idea of the homogenization methods is to compute homogenized coefficients (effective properties) by solving cell problems and derive macroscopic equations on a coarse grid. This significantly reduces computational costs and speeds up calculations. However, in the case of high-contrast heterogeneous media, the classical homogenization method may not be sufficient because it provides only one effective coefficient at a macroscale point. For accurate modeling, the coarse-grid formulation needs multiple homogenized coefficients. Multicontinuum approaches define different average states (continua) and introduce several effective properties per coarse-grid node. There are many works devoted to developing multicontinuum approaches for different applications [20, 21, 22, 23]. Among them, one can mention a recently presented multicontinuum homogenization method [24, 25, 26], which allows us to rigorously derive multicontinuum models. The main idea of the multicontinuum homogenization method is to derive a macroscopic model by formulating constraint cell problems and obtaining multicontinuum expansions. This method has already been successfully applied to different problems [27, 28, 29, 30].

Note that one can also apply various multiscale methods to numerically solve problems with high-contrast properties, such as the Multiscale Finite Volume Method (MsFVM) [31, 32, 33], the Multiscale Finite Element Method (MsFEM) [34, 35, 36, 37], the Generalized Multiscale Finite Element Method (GMsFEM) [38, 39, 40, 41, 42] and the Constraint Energy Minimizing Generalized Multiscale Finite Element Method (CEM-GMsFEM) [43, 44, 45]. In these multiscale approaches, one constructs multiscale basis functions by solving local problems. Then, the computed basis functions are used to obtain the coarse-grid problem. The multiscale methods demonstrated high efficiency in solving time-fractional derivative problems with heterogeneous coefficients [46, 47, 48]. However, the obtained coarse-grid models are discrete and not in the form of macroscopic laws.

In this paper, we use the multicontinuum homogenization to the time-fractional diffusion-wave equation with high-contrast coefficient κ . The main challenges lie in formulating constraint cell problems, deriving the multicontinuum model, and discretizing the time-fractional derivative. We formulate and solve constraint cell problems that account for different averages and gradient effects. Using the cell problems' solutions, we obtain the multicontinuum expansions and substitute them into the variational formulation of the time-fractional diffusion-wave equation. Then, we derive a general multicontinuum model that includes macroscopic variables and homogenized coefficients. For temporal discretization, we apply the fully discrete scheme [11] that can efficiently handle time-fractional derivatives. To validate the efficiency of the proposed approach, we consider two-dimensional model problems with high-contrast coefficients. We consider various orders of time-fractional derivatives, including the mixed case, where we have different orders in different continua. The numerical results show that the proposed multicontinuum approach provides high accuracy and can handle various heterogeneity types and time-fractional derivatives orders.

Our main contributions in this work are as follows. First, we obtain a macroscopic model for a

time-fractional equation with mixed time derivatives and zero-order spatial derivatives. Second, we derive the multicontinuum time-fractional diffusion-wave model using the multicontinuum homogenization approach. Finally, we present numerical results to demonstrate the efficiency of the proposed approach.

The rest of the paper is organized as follows. In the next section, we present preliminaries and derive the multicontinuum model for the time-fractional zero-order equations. Section 3 is devoted to the derivation of the multicontinuum time-fractional diffusion-wave model. In Section 4, we present numerical experiments to test the efficiency of our proposed approach. Finally, we present conclusions in Section 5.

2 Preliminaries

In this section, we present preliminaries. First, we describe the fully discrete scheme used for approximating time-fractional derivatives. Then, we present the derivation of the multicontinuum equations for the case with mixed time-fractional derivatives and zero-order spatial terms using the multicontinuum homogenization method.

2.1 Time-fractional diffusion-wave equation

Let us consider the following time-fractional diffusion-wave equation (TFDWE),

$$\frac{\partial^\alpha u}{\partial t^\alpha} - \nabla \cdot (\kappa \nabla u) = f, \quad \Omega \times [0, T], \quad (1)$$

with the initial conditions

$$u(x, 0) = \phi(x), \quad \frac{\partial u(x, 0)}{\partial t} = \psi(x), \quad (2)$$

and the boundary conditions

$$u(0, t) = \varphi_1(x), \quad u(L, t) = \varphi_2(x), \quad t > 0, \quad (3)$$

where $\kappa = \kappa(x)$ is a heterogeneous coefficient such that $\eta = \max \kappa / \min \kappa \gg 1$, $\phi(x)$, $\psi(x)$, $\varphi_1(x)$, and $\varphi_2(x)$ are known functions, $f(x, t)$ is a known source term, T is the final time, Ω is a bounded domain in R^d ($d = 1, 2, \dots$) with boundary $\partial\Omega$, and

$$\frac{\partial^\alpha u}{\partial t^\alpha} = \frac{1}{\Gamma(2-\alpha)} \int_0^t \frac{\partial^2 u(x, s)}{\partial s^2} \frac{ds}{(t-s)^{\alpha-1}}, \quad 1 < \alpha < 2$$

is the Caputo fractional derivative of order α with Γ denoting the gamma function. Note that if $\alpha = 1$, equation (1) represents a traditional diffusion equation. When $\alpha = 2$, equation (1) is considered as a traditional wave equation. For $1 < \alpha < 2$, equation (1) is known as the time-fractional diffusion-wave equation, since it can describe intermediate processes between diffusion ($\alpha = 1$) and wave ($\alpha = 2$) phenomena.

To approximate the time-fractional derivative $\frac{\partial^\alpha u}{\partial t^\alpha}$, we first decompose the time interval $[0, T]$ evenly into N_t time subintervals (t_n, t_{n+1}) , $n = 0, 1, \dots, N_t - 1$, with the time step size $\tau = \frac{T}{N_t}$. For ease of statement, we can suppose that $u(\cdot, t_n) = \{u^n | 0 \leq n \leq N_t\}$ is a grid function on Ω , where $t_n = n\tau, \tau > 0$. Let us introduce the following notations

$$\delta_t u^{n-\frac{1}{2}} = \frac{1}{\tau}(u^n - u^{n-1}), \quad u^{n-\frac{1}{2}} = \frac{1}{2}(u^n + u^{n-1}),$$

where $u^{n-\frac{1}{2}}$ is the difference quotient of u at the temporal points t_n and t_{n-1} , and $u^{n-\frac{1}{2}}$ represents an average of u on these two points.

According to the fully discrete scheme in [11], we can approximate the time-fractional derivative as follows

$$\frac{\partial^\alpha u}{\partial t^\alpha} \approx \frac{\tau^{1-\alpha}}{\Gamma(3-\alpha)} \left[a_0 \delta_t u^{n-\frac{1}{2}} - \sum_{k=1}^{n-1} (a_{n-k-1} - a_{n-k}) \delta_t u^{k-\frac{1}{2}} - a_{n-1} \psi \right] \quad (4)$$

where $a_k = (k+1)^{2-\alpha} - k^{2-\alpha}$ ($k > 0$). Sun and Wu [11] proved the solvability, unconditional stability, and L_∞ convergence by the energy method. Note that the convergence order for time is $O(\tau^{3-\alpha})$.

For spatial approximation, we can consider the finite element approximation of (1). The weak formulation of (1) reads: Find $u^n \in H_0^1(\Omega)$ such that for all $v \in H_0^1(\Omega)$

$$\begin{aligned} & \frac{\tau^{1-\alpha}}{\Gamma(3-\alpha)} \left[a_0 (\delta_t u^{n-\frac{1}{2}}, v) - \sum_{k=1}^{n-1} (a_{n-k-1} - a_{n-k}) (\delta_t u^{k-\frac{1}{2}}, v) - a_{n-1} (\psi, v) \right] \\ & = -(\kappa \nabla u^{n-\frac{1}{2}}, \nabla v) + (f^{n-\frac{1}{2}}, v), \quad 1 \leq n \leq N_t, \end{aligned} \quad (5)$$

where $f^{n-\frac{1}{2}} = f(\cdot, \frac{t_n+t_{n-1}}{2})$.

2.2 Multicontinuum time-fractional zero-order equations

Let us consider the following time-fractional equation with a zero-order spatial term

$$\frac{\partial^{\alpha_k} u}{\partial t^{\alpha_k}} \psi_k + A(x)u(x) = f(x), \quad 1 < \alpha_k < 2, \quad (6)$$

where $A(x)$ is a scalar function with multiple scales and high contrast symbol k is the Einstein summation convention. For example, let A be a periodic function comprises two different regions with highly diverse coefficients. We assume ψ_k is the characteristic function for the region Ω_k , called the k th continua ($k = 1, \dots, N$). Here, α_k are distinct time derivative orders in different regions.

Assume that the problem is defined on a computational domain Ω . Moreover, we divide the computational domain Ω into coarse blocks ω 's. Suppose that we can define a representative volume (RVE) R_ω within each ω , i.e., coarse-grid elements ω contain RVEs. Next, we introduce an oversampled RVE R_ω^+ , which is composed of several RVEs R_ω^p , where $R_\omega^{p_0} = R_\omega$. We depict the relationships of Ω , ω , R_ω^+ , and R_ω in Figure 1.

There are some following points to notice:

- Each R_ω can represent the whole coarse-grid element ω in terms of heterogeneities;
- Each R_ω contains N continua (components). Moreover, in each R_ω , we define the characteristic function ψ_j for continuum j , i.e., $\psi_j = \delta_{ij}$ within continuum i , where

$$\delta_{ij} = \begin{cases} 1, & i = j, \\ 0, & i \neq j. \end{cases}$$

We define the expansion of u in each RVE as

$$u = \phi_i U_i, \quad (7)$$

where ϕ_i is a microscopic function, and $U_i(x)$ is a smooth macroscopic function for each continuum i . Here, we use the Einstein summation convention. To obtain ϕ_i , we introduce the following cell problems in each RVE R_ω . Note that we apply y dependence to represent microscopic properties.

$$\begin{aligned} & A(y)\phi_i(y) = D_{ij}\psi_j, \quad \text{in } R_\omega, \\ & \int_{R_\omega} \phi_i \psi_j = \delta_{ij} \int_{R_\omega} \psi_j, \quad \text{for each } j, \end{aligned} \quad (8)$$

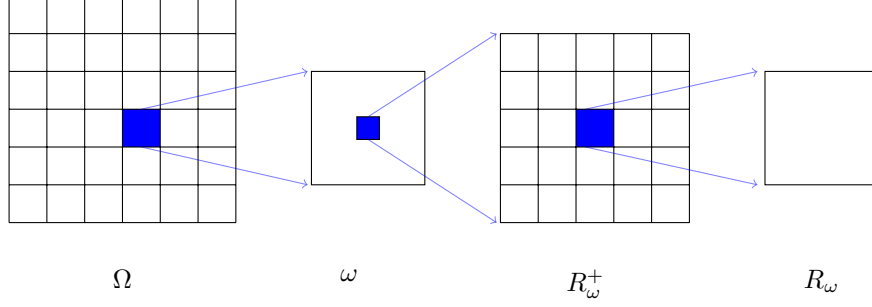


Figure 1: Illustration of computation domain Ω , coarse block ω , RVE R_ω , and the oversampling domain R_ω^+ .

where $D_{ij}\psi_j = C_i\psi_i$ (D_{ij} are constants). One can see that $A\phi_i = C_i\psi_i$ and

$$C_j = \frac{\int_{R_\omega} \psi_j}{\int_{R_\omega} \psi_j^2 A^{-1}}.$$

Next, let us derive multicontinuum equations for U_i . We first write a weak formulation of (6) for an arbitrary test function v

$$\begin{aligned} \int_{\Omega} f v &= \int_{\Omega} \frac{\partial^{\alpha_k} u(x)}{\partial t^{\alpha_k}} \psi_k v(x) + \int_{\Omega} A(x) u(x) v(x) \\ &= \sum_{\omega} \int_{\omega} \frac{\partial^{\alpha_k} u(x)}{\partial t^{\alpha_k}} \psi_k v(x) + \sum_{\omega} \int_{\omega} A(x) u(x) v(x) \\ &\approx \sum_{\omega} \frac{|\omega|}{|R_\omega|} \int_{R_\omega} \frac{\partial^{\alpha_k} u(y)}{\partial t^{\alpha_k}} \psi_k v(y) + \sum_{\omega} \frac{|\omega|}{|R_\omega|} \int_{R_\omega} A(y) u(y) v(y). \end{aligned} \quad (9)$$

Next, we substitute u from (7) into the equation (9), and (utilizing $v = \phi_i V_i$) we can approximate the first term of (9) as follows

$$\begin{aligned} \int_{R_\omega} \frac{\partial^{\alpha_k} u(y)}{\partial t^{\alpha_k}} \psi_k v(y) &\approx \frac{\partial^{\alpha_k} U_i(x_\omega)}{\partial t^{\alpha_k}} V_j(x_\omega) \int_{R_\omega} \psi_k \phi_i(y) \phi_j(y) \\ &= \frac{\partial^{\alpha_k} U_i(x_\omega)}{\partial t^{\alpha_k}} V_j(x_\omega) \int_{R_\omega} \psi_k \frac{C_i C_j}{A(y) A(y)} \psi_i \psi_j, \end{aligned} \quad (10)$$

where x_ω is a mid-point of R_ω . We will omit the microscopic dependence of macroscale variables (e.g., U_i) and merely apply U_i symbol

$$\int_{R_\omega} \frac{\partial^{\alpha_k} u(y)}{\partial t^{\alpha_k}} \psi_k v(y) = \frac{\partial^{\alpha_k} U_i}{\partial t^{\alpha_k}} V_j \int_{R_\omega} \psi_k \frac{C_i C_j}{A(y) A(y)} \psi_i \psi_j. \quad (11)$$

Let us denote

$$\gamma_{ijk} = \int_{R_\omega} \psi_k \frac{C_i C_j}{A(y) A(y)} \psi_i \psi_j. \quad (12)$$

Note that γ_{ijk} takes non-zero values only in the case of $i = j = k$. Therefore, we can represent it as follows

$$\gamma_i = C_i^2 \int_{R_\omega} \frac{\psi_i^3}{A^2}. \quad (13)$$

The second term of (9) is approximated in a similar way

$$\begin{aligned} \int_{R_\omega} A(y)u(y)v(x) &\approx U_i V_j \int_{R_\omega} A(y)\phi_i(y)\phi_j(y) \\ &= U_i V_j \beta_{ij}, \end{aligned} \quad (14)$$

where

$$\begin{aligned} \beta_{ij} &= \int_{R_\omega} A(y)\phi_i(y)\phi_j(y) \\ &= C_i \int_{R_\omega} \psi_i \phi_j \\ &= C_i \delta_{ij} \int_{R_\omega} \psi_i. \end{aligned} \quad (15)$$

One can see that β_{ij} takes non-zero values only in the case of $i = j$. Thus, we can represent it in the following form

$$\beta_i = C_i \int_{R_\omega} \psi_i. \quad (16)$$

From the above, we can obtain the following macroscopic equations for (6)

$$\gamma_{ijk} \frac{\partial^{\alpha_k} U_i}{\partial t^{\alpha_k}} + \beta_{ij} U_i = b_j, \quad j = 1, \dots, N, \quad 1 < \alpha < 2, \quad (17)$$

where $b_j = \int_{R_\omega} f \phi_j$.

Considering that γ and α are diagonal matrices, we have

$$\gamma_i \frac{\partial^{\alpha_i} U_i}{\partial t^{\alpha_i}} + \beta_i U_i = b_i, \quad i = 1, \dots, N, \quad 1 < \alpha < 2. \quad (18)$$

One can see that the obtained macroscopic model is described by separate (not coupled) equations for each continuum.

3 Multicontinuum homogenization

In this section, we derive the multicontinuum time-fractional diffusion-wave model using the multicontinuum homogenization method. We formulate constraint cell problems by imposing constraints for averages and gradient effects. These cell problems are defined in oversampled domains to reduce boundary effects. By applying the expansions to the variational formula, we can rigorously derive the multicontinuum model. This section consists of two subsections. In the first subsection, we present the derivation for the regular time-fractional diffusion-wave equation. The second subsection considers the case with mixed time derivatives, where we have different time derivative orders in different continua.

3.1 Multicontinuum time-fractional diffusion-wave model

Let us consider the following variational formulation of the time-fractional diffusion-wave equation (1)

$$\int_{\Omega} \frac{\partial^{\alpha} u}{\partial t^{\alpha}} v + \int_{\Omega} \kappa \nabla u \cdot \nabla v = \int_{\Omega} f v, \quad 1 < \alpha < 2, \quad \forall v \in H_0^1(\Omega). \quad (19)$$

In the multicontinuum homogenization method, we suppose that we can define characteristic functions of continua in each RVE R_ω such that

$$U_i(x_\omega) \approx \frac{\int_{R_\omega} u \psi_i}{\int_{R_\omega} \psi_i}.$$

We assume that $U_i(x)$ are smooth functions denoting macroscopic variables, where x_ω is a middle point of R_ω . Next, we present the derivation of the multicontinuum model for the time-fractional diffusion-wave equation.

Expansion.

We expand the solution u over macroscopic variables

$$u = \phi_i U_i + \phi_i^m \nabla_m U_i + \phi_i^{mn} \nabla_{mn}^2 U_i + \dots, \quad (20)$$

where $\nabla_m = \frac{\partial}{\partial x_m}$, $\nabla_{mn}^2 = \frac{\partial^2}{\partial x_m \partial x_n}$. In this expansion, U_i is the macroscopic quantity representing the average of the solution within i -th continuum, and $\phi_i, \phi_i^m, \phi_i^{mn}, \dots$ are auxiliary basis functions defined as the solutions of cell problems. For sake of simplicity, we will neglect the terms after the second term and only use the first two terms in (20). Therefore, we can rewrite the expansion of u as

$$u \approx \phi_i U_i + \phi_i^m \nabla_m U_i, \quad (21)$$

where U_i can be considered as a limit of $\int_{R_\omega} u \psi_i / \int_{R_\omega} \psi_i$.

Cell problems.

Next, we introduce cell problems for auxiliary basis functions ϕ_i and ϕ_i^m . These constrained cell problems are formulated by using Lagrange multipliers. To avoid boundary effects, we define the cell problems in oversampled regions R_ω^+ , consisting of R_ω^p . We can minimize the local solution subject to different constraints [25, 24].

The first cell problem considers different averages in each continuum and stands for the constants in the average behavior

$$\begin{aligned} \int_{R_\omega^+} \kappa \nabla \phi_i \cdot \nabla v - \sum_{j,p} \frac{\beta_{ij}^p}{\int_{R_\omega^p} \psi_j^p} \int_{R_\omega^p} \psi_j^p v &= 0, \\ \int_{R_\omega^p} \phi_i \psi_j^p &= \delta_{ij} \int_{R_\omega^p} \psi_j^p. \end{aligned} \quad (22)$$

The second cell problem considers gradient effects and imposes constraints to stand for the linear functions in the average behavior of each continuum

$$\begin{aligned} \int_{R_\omega^+} \kappa \nabla \phi_i^m \cdot \nabla v - \sum_{j,p} \frac{\beta_{ij}^{mp}}{\int_{R_\omega^p} \psi_j^p} \int_{R_\omega^p} \psi_j^p v &= 0, \\ \int_{R_\omega^p} \phi_i^m \psi_j^p &= \delta_{ij} \int_{R_\omega^p} (x_m - c_{mj}) \psi_j^p, \end{aligned} \quad (23)$$

where c_{mj} satisfy $\int_{R_\omega^p} (x_m - c_{mj}) \psi_j^p = 0$.

Note that we have the following estimates for ϕ_i and ϕ_i^m [24]

$$\begin{aligned} \|\phi_i\| &= O(1), \quad \|\nabla \phi_i\| = O\left(\frac{1}{\epsilon}\right), \\ \|\phi_i^m\| &= O(\epsilon), \quad \|\nabla \phi_i^m\| = O(1), \end{aligned} \quad (24)$$

where ϵ is a diameter of RVE.

Integral localization.

Utilizing the RVE concept, for any $v \in H_0^1$, we can get

$$\begin{aligned} \int_{\Omega} f v &= \int_{\Omega} \frac{\partial^\alpha u}{\partial t^\alpha} v + \int_{\Omega} \kappa \nabla u \cdot \nabla v \\ &= \sum_{\omega} \int_{\omega} \frac{\partial^\alpha u}{\partial t^\alpha} v + \sum_{\omega} \int_{\omega} \kappa \nabla u \cdot \nabla v \\ &\approx \sum_{\omega} \frac{|\omega|}{|R_\omega|} \int_{R_\omega} \frac{\partial^\alpha u}{\partial t^\alpha} v + \sum_{\omega} \frac{|\omega|}{|R_\omega|} \int_{R_\omega} \kappa \nabla u \cdot \nabla v, \end{aligned} \quad (25)$$

where we assume that integrated average over RVE R_ω can represent the whole coarse block ω in terms of heterogeneities.

Substitution into the variational formulation.

We can expand u and v as follows

$$\begin{aligned} u &\approx \phi_i U_i + \phi_i^m \nabla_m U_i, \\ v &\approx \phi_j V_j + \phi_j^n \nabla_n V_j, \end{aligned} \quad (26)$$

where U_i and V_j are smooth macroscopic functions.

Substituting (26) into (25), we can obtain the following approximation of the variational formulation

$$\begin{aligned} &\sum_{R_\omega} \frac{|\omega|}{|R_\omega|} \left(\int_{R_\omega} \frac{\partial^\alpha (\phi_i U_i + \phi_i^m \nabla_m U_i)}{\partial t^\alpha} (\phi_j V_j + \phi_j^n \nabla_n V_j) + \right. \\ &\sum_{R_\omega} \frac{|\omega|}{|R_\omega|} \int_{R_\omega} \kappa \nabla (\phi_i U_i + \phi_i^m \nabla_m U_i) \cdot \nabla (\phi_j V_j + \phi_j^n \nabla_n V_j) = \\ &\left. \sum_{R_\omega} \frac{|\omega|}{|R_\omega|} \int_{R_\omega} \{(f, \phi_j V_j) + (f, \phi_j^n \nabla_n V_j)\}. \right. \end{aligned} \quad (27)$$

Macroscopic model.

Due to the smoothness of the macroscopic variables, the variations of U_i and $\nabla_m U_i$ are small compared to the variations of ϕ_i and ϕ_i^m . Therefore, we assume $\int_{R_\omega} \kappa \nabla (\phi_i U_i) \cdot \nabla v \approx \int_{R_\omega} \kappa \nabla (\phi_i) U_i \cdot \nabla v$ and $\int_{R_\omega} \kappa \nabla (\phi_i^m \nabla_m U_i) \cdot \nabla v \approx \int_{R_\omega} \kappa \nabla (\phi_i^m) \nabla_m U_i \cdot \nabla v$. As before (in the zero-order case), we take the macroscopic variables out of the integrals over R_ω .

We can approximate the first term on the left-hand side of (27) as follows

$$\begin{aligned} &\sum_{R_\omega} \frac{|\omega|}{|R_\omega|} \left(\int_{R_\omega} \frac{\partial^\alpha (\phi_i U_i + \phi_i^m \nabla_m U_i)}{\partial t^\alpha} (\phi_j V_j + \phi_j^n \nabla_n V_j) \right) = \\ &\sum_{\omega} \frac{|\omega|}{|R_\omega|} \left(\int_{R_\omega} \phi_i \phi_j \frac{\partial^\alpha}{\partial t^\alpha} U_i V_j + \sum_{\omega} \frac{|\omega|}{|R_\omega|} \left(\int_{R_\omega} \phi_i \phi_j^n \frac{\partial^\alpha}{\partial t^\alpha} U_i \nabla_n V_j + \right. \right. \\ &\sum_{\omega} \frac{|\omega|}{|R_\omega|} \left(\int_{R_\omega} \phi_i^m \phi_j \frac{\partial^\alpha}{\partial t^\alpha} \nabla_m U_i V_j + \sum_{\omega} \frac{|\omega|}{|R_\omega|} \left(\int_{R_\omega} \phi_i^m \phi_j^n \frac{\partial^\alpha}{\partial t^\alpha} \nabla_m U_i \nabla_n V_j \right. \right. \\ &\left. \left. \approx \sum_{\omega} \frac{|\omega|}{|R_\omega|} \left(\int_{R_\omega} \phi_i \phi_j \frac{\partial^\alpha}{\partial t^\alpha} U_i V_j. \right. \right. \end{aligned} \quad (28)$$

In addition, let us introduce the following notations corresponding to the coefficients of the terms in (28)

$$\begin{aligned} C_{ji} &= \int_{R_\omega} \phi_i \phi_j, & C_{ji}^n &= \int_{R_\omega} \phi_i \phi_j^n, \\ C_{ji}^m &= \int_{R_\omega} \phi_i^m \phi_j, & C_{ji}^{mn} &= \int_{R_\omega} \phi_i^m \phi_j^n. \end{aligned}$$

Note that in the last step of (28), we cancel the second, third, and fourth terms. The reason for these is that ϕ_j^n is of the order $O(\epsilon)$, while ϕ_j 's order is of the order $O(1)$.

The second term on the left-hand side of (27) can be written as

$$\begin{aligned} &\sum_{R_\omega} \frac{|\omega|}{|R_\omega|} \int_{R_\omega} \kappa \nabla (\phi_i U_i + \phi_i^m \nabla_m U_i) \cdot \nabla (\phi_j V_j + \phi_j^n \nabla_n V_j) = \\ &\sum_{R_\omega} \frac{|\omega|}{|R_\omega|} \left\{ \left(\int_{R_\omega} \kappa \nabla \phi_i \cdot \nabla \phi_j \right) U_i V_j + \left(\int_{R_\omega} \kappa \nabla \phi_i \cdot \nabla \phi_j^n \right) U_i \nabla_n V_j \right\} + \\ &\sum_{R_\omega} \frac{|\omega|}{|R_\omega|} \left\{ \left(\int_{R_\omega} \kappa \nabla \phi_i^m \cdot \nabla \phi_j \right) \nabla_m U_i V_j + \left(\int_{R_\omega} \kappa \nabla \phi_i^m \cdot \nabla \phi_j^n \right) \nabla_m U_i \nabla_n V_j \right\}. \end{aligned} \quad (29)$$

Accordingly, we introduce the following notations

$$\begin{aligned} B_{ji} &= \int_{R_\omega} \kappa \nabla \phi_i \cdot \nabla \phi_j, & B_{ji}^n &= \int_{R_\omega} \kappa \nabla \phi_i \cdot \nabla \phi_j^n, \\ B_{ji}^m &= \int_{R_\omega} \kappa \nabla \phi_i^m \cdot \nabla \phi_j, & B_{ji}^{mn} &= \int_{R_\omega} \kappa \nabla \phi_i^m \cdot \nabla \phi_j^n. \end{aligned}$$

Applying the formula (24), we can obtain the following estimates for B_{ji} , C_{ji} , B_{ji}^m , and B_{ji}^{mn}

$$B_{ji} = O\left(\frac{|R_\omega|}{\epsilon^2}\right), \quad B_{ji}^m = O\left(\frac{|R_\omega|}{\epsilon}\right), \quad B_{ji}^{mn} = O(|R_\omega|), \quad C_{ji} = O(|R_\omega|).$$

Then, we can define the scaled effective properties as follows

$$\widehat{B}_{ji} = \frac{\epsilon^2}{|R_\omega|} B_{ji}, \quad \widehat{B}_{ji}^m = \frac{\epsilon}{|R_\omega|} B_{ji}^m, \quad \widehat{B}_{ji}^{mn} = \frac{1}{|R_\omega|} B_{ji}^{mn}, \quad \widehat{C}_{ji} = \frac{1}{|R_\omega|} C_{ji}. \quad (30)$$

Hence, with these scalings, we can get

$$\begin{aligned} \int_{\Omega} \frac{\partial^\alpha u}{\partial t^\alpha} v + \int_{\Omega} \kappa \nabla u \cdot \nabla v &\approx \int_{\Omega} \widehat{C}_{ji} \frac{\partial^\alpha U_i}{\partial t^\alpha} V_j + \int_{\Omega} \widehat{B}_{ji}^{mn} \nabla_m U_i \nabla_n V_j + \\ \frac{1}{\epsilon} \int_{\Omega} \widehat{B}_{ji}^m \nabla_m U_i V_j + \frac{1}{\epsilon} \int_{\Omega} \widehat{B}_{ji}^m U_i \nabla_m V_j + \frac{1}{\epsilon^2} \int_{\Omega} \widehat{B}_{ji} U_i V_j. \end{aligned} \quad (31)$$

By utilizing the integration by parts, one can show that the sum of the third and fourth terms on the right-hand side of (31) is negligible [24].

Thus, we obtain the following multicontinuum time-fractional diffusion-wave model (in strong form)

$$\widehat{C}_{ji} \frac{\partial^\alpha U_i}{\partial t^\alpha} - \nabla_n (\widehat{B}_{ji}^{mn} \nabla_m U_i) + \frac{1}{\epsilon^2} \widehat{B}_{ji} U_i = f_j. \quad (32)$$

where $f_j = \frac{1}{|R_\omega|} \int_{R_\omega} f \phi_j$. One can see that the reaction terms are dominant unless we have large diffusions, i.e., high contrast.

3.2 Multicontinuum time-fractional diffusion-wave model with mixed time derivatives

Let us now consider the following time-fractional diffusion-wave equation with mixed time derivatives

$$\frac{\partial^{\alpha_p} u}{\partial t^{\alpha_p}} \psi_p - \nabla \cdot (\kappa \nabla u) = f, \quad 1 < \alpha_p < 2, \quad \Omega \times [0, T], \quad (33)$$

where κ is a high-contrast heterogeneous coefficient, and ψ_p is the characteristic function for the subdomain Ω_p , i.e., the p th continuum ($p = 1, \dots, N$). Here, we suppose the Einstein summation convention over p indices.

Applying the RVE, we first obtain a weak form of (33) for an arbitrary test function $v \in H_0^1$ as follows

$$\begin{aligned} \int_{\Omega} f v &= \int_{\Omega} \frac{\partial^{\alpha_p} u}{\partial t^{\alpha_p}} \psi_p v + \int_{\Omega} \kappa \nabla u \cdot \nabla v \\ &= \sum_{\omega} \int_{\omega} \frac{\partial^{\alpha_p} u}{\partial t^{\alpha_p}} \psi_p v + \sum_{\omega} \int_{\omega} \kappa \nabla u \cdot \nabla v \\ &\approx \sum_{\omega} \frac{|\omega|}{|R_\omega|} \int_{R_\omega} \frac{\partial^{\alpha_p} u}{\partial t^{\alpha_p}} \psi_p v + \sum_{\omega} \frac{|\omega|}{|R_\omega|} \int_{R_\omega} \kappa \nabla u \cdot \nabla v, \end{aligned} \quad (34)$$

The cell problems are the same as for the regular time-fractional diffusion-wave equation. Thus, we can define the following multicontinuum expansion of u and v

$$\begin{aligned}
u &\approx \phi_i U_i + \phi_i^m \nabla_m U_i, \\
v &\approx \phi_j V_j + \phi_j^n \nabla_n V_j.
\end{aligned} \tag{35}$$

Then, we can approximate (34) as follows

$$\begin{aligned}
&\sum_{R_\omega} \frac{|\omega|}{|R_\omega|} \left(\int_{R_\omega} \frac{\partial^{\alpha_p} (\phi_i U_i + \phi_i^m \nabla_m U_i)}{\partial t^{\alpha_p}} \psi_p (\phi_j V_j + \phi_j^n \nabla_n V_j) + \right. \\
&\sum_{R_\omega} \frac{|\omega|}{|R_\omega|} \int_{R_\omega} \nabla (\phi_i U_i + \phi_i^m \nabla_m U_i) \cdot \nabla (\phi_j V_j + \phi_j^n \nabla_n V_j) = \\
&\left. \sum_{R_\omega} \frac{|\omega|}{|R_\omega|} \{ (f, \phi_j V_j) + (f, \phi_j^n \nabla_n V_j) \}. \right.
\end{aligned} \tag{36}$$

The first term on the left-hand side of (36) can be rewritten in the following form (for brevity, we will omit $\sum_\omega \frac{|\omega|}{|R_\omega|}$)

$$\begin{aligned}
&\int_{R_\omega} \frac{\partial^{\alpha_p} (\phi_i U_i + \phi_i^m \nabla_m U_i)}{\partial t^{\alpha_p}} \psi_p (\phi_j V_j + \phi_j^n \nabla_n V_j) \\
&= C_{jip}^{\alpha_p} \frac{\partial^{\alpha_p}}{\partial t^{\alpha_p}} U_i V_j + C_{jip}^n \frac{\partial^{\alpha_p}}{\partial t^{\alpha_p}} U_i \nabla_n V_j + C_{jip}^m \frac{\partial^{\alpha_p}}{\partial t^{\alpha_p}} \nabla_m U_i V_j + C_{jip}^{mn} \frac{\partial^{\alpha_p}}{\partial t^{\alpha_p}} \nabla_m U_i \nabla_n V_j \\
&\approx C_{jip}^{\alpha_p} \frac{\partial^{\alpha_p}}{\partial t^{\alpha_p}} U_i V_j.
\end{aligned} \tag{37}$$

where

$$\begin{aligned}
C_{jip} &= \int_{R_\omega} \phi_i \phi_j \psi_p, & C_{jip}^n &= \int_{R_\omega} \phi_i \phi_j^n \psi_p, \\
C_{jip}^m &= \int_{R_\omega} \phi_i^m \phi_j \psi_p, & C_{jip}^{mn} &= \int_{R_\omega} \phi_i^m \phi_j^n \psi_p.
\end{aligned}$$

The second term on the left-hand side of (36) is the same as in the regular case. Therefore, we can write it as follows

$$\int_{R_\omega} \kappa \nabla u \cdot \nabla v \approx \int_{R_\omega} B_{ji} U_i V_j + \int_{R_\omega} B_{ji}^n U_i \nabla_n V_j + \int_{R_\omega} B_{ji}^m \nabla_m U_i V_j + \int_{R_\omega} B_{ji}^{mn} \nabla_m U_i \nabla_n V_j, \tag{38}$$

where

$$\begin{aligned}
B_{ji} &= \int_{R_\omega} \kappa \nabla \phi_i \cdot \nabla \phi_j, & B_{ji}^n &= \int_{R_\omega} \kappa \nabla \phi_i \cdot \nabla \phi_j^n, \\
B_{ji}^m &= \int_{R_\omega} \kappa \nabla \phi_i^m \cdot \nabla \phi_j, & B_{ji}^{mn} &= \int_{R_\omega} \kappa \nabla \phi_i^m \cdot \nabla \phi_j^n.
\end{aligned}$$

Note that we can obtain the estimate $C_{jip} = O(|R_\omega|)$. Then, we have the following scaled effective property $\widehat{C}_{jip} = \frac{1}{|R_\omega|} C_{jip}$. Eventually, we obtain the following multicontinuum model (in strong form)

$$\widehat{C}_{jip} \frac{\partial^{\alpha_p} U_i}{\partial t^{\alpha_p}} - \nabla_n (\widehat{B}_{ji}^{mn} \nabla_m U_i) + \frac{1}{\epsilon^2} \widehat{B}_{ji} U_i = f_j. \tag{39}$$

Thus, each equation contains a linear combination of time-fractional derivatives of all orders.

4 Numerical results

In this section, we conduct numerical experiments to check the efficiency of the proposed multicontinuum homogenization approach. For this purpose, we consider two-dimensional model problems in different high-contrast heterogeneous media. We consider various time-fractional derivative orders, including the mixed derivatives case.

As a computational domain, we set $\Omega = \Omega_1 \cup \Omega_2 = [0, 1] \times [0, 1]$, where Ω_1 is a low conductive region, and Ω_2 is a highly conductive region. To construct a fine grid, we divide Ω into 400×400 square blocks. We partition Ω evenly into $M \times M$ square blocks (each divided into two triangles) to construct a coarse grid. Therefore, the coarse grid size is $H = 1/M$. For sake of simplicity, each whole coarse-grid block will be considered as an RVE itself. The oversampled RVE R_ω^+ is constructed as an extension of the target block by l layers of coarse-grid blocks. To estimate the accuracy of the proposed approach, we use the following relative L^2 -error norms

$$e^{(i)}(t) = \sqrt{\frac{\sum_K \left| \frac{1}{|K|} \int_K U_i(x, t) dx - \frac{1}{|K \cap \Omega_i|} \int_{K \cap \Omega_i} u(x, t) dx \right|^2}{\sum_K \left| \frac{1}{|K \cap \Omega_i|} \int_{K \cap \Omega_i} u(x, t) dx \right|^2}}, \quad (40)$$

where $i = 1, 2$, and K denotes the RVE, which is taken to be ω .

We consider two coarse grid sizes: $1/20$ and $1/40$. We determine the number of oversampling layers l using the formula $l = \lceil -2 \log(H) \rceil$ [24]. Hence, we have $l = 6$ for $H = 1/20$ and $l = 8$ for $H = 1/40$. We utilize the finite element method with standard piece-wise linear basis functions for spatial approximation of both fine-grid and coarse-grid models. For temporal approximation, we apply proposed the fully discrete scheme (4). We take the time step $\tau = 0.02$ and set the final time $T = 1$.

The numerical implementation is based on the open-source computational package FEniCS [49]. The visualization of the obtained numerical results was performed using the ParaView software [50].

4.1 Example 1: Crossed field

First, let us consider the heterogeneous coefficient κ with a crossed structure (see Figure 2). Moreover, we suppose that κ possesses a high contrast and can be represented in the following form

$$\kappa(x) = \begin{cases} 10^{-4}, & x \in \Omega_1, \\ 1, & x \in \Omega_2. \end{cases} \quad (41)$$

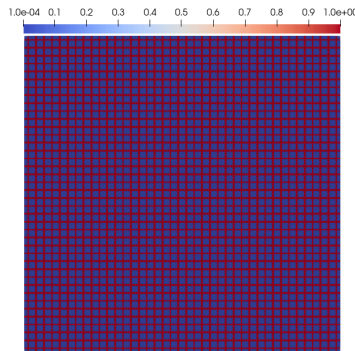


Figure 2: The coefficient κ (Ω_1 : blue regions; Ω_2 : red regions). Crossed field.

The source term f is given as $f(x) = e^{-40((x_1-0.5)^2+(x_2-0.5)^2)}$ for any $x = (x_1, x_2) \in \Omega$. We set the initial condition $u_0 = u(x, 0) = 0$, and the following Dirichlet boundary condition

$$u(x, t) = 0, \quad x \in \partial\Omega. \quad (42)$$

We consider two cases of time-fractional derivative orders. In the first case, we set the same orders for both continua (regions). The second case corresponds to the mixed time derivatives, where we have different orders in different continua.

4.1.1 Case 1: Regular time derivatives

Let us consider the case with the same time-fractional derivatives in both continua. Figure 3 depicts distributions of the fine-grid solution for $\alpha = 1.5$ at different time steps. One can see how the solution field grows from the middle of the domain due to the source term. We can observe the high-contrast diffusion coefficient's influence on the distribution of the solution. The solution field propagates faster in the high-conductive channels while it moves slowly in the low-conductive subregions. In general, the obtained solution corresponds to the simulated process.

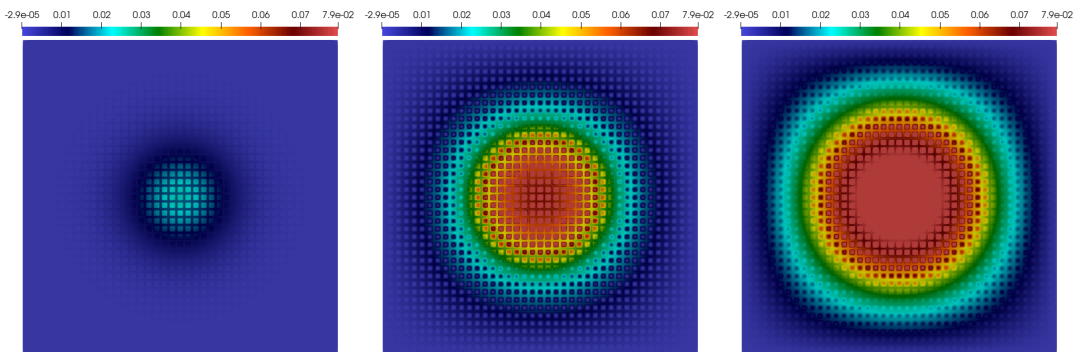


Figure 3: The fine-grid reference solution with $\alpha = 1.5$ at $t = 0.1, 0.5, 1$ for Case 1 in Example 1 (from left to right).

Figures 4-5 presents distributions of the average solutions with $H = 1/40$ in Ω_1 and Ω_2 subregions, respectively. From top to bottom, we depict the reference and multiscale average solutions. One can see that the solutions are very similar, which indicates that our proposed multicontinuum approach can approximate the reference solution with high accuracy. In terms of the simulated process, we observe that the average solution field in Ω_2 (U_1) diffuses much faster than those in Ω_2 (U_2), as expected. Moreover, one can see that the propagation process is isotropic.

Next, let us consider the relative errors of the multiscale solutions. Tables 1, 2, and 3 present the relative L^2 errors at different time steps for $\alpha = 1.1$, $\alpha = 1.5$, and $\alpha = 1.9$, respectively. In all the tables, we present the errors for $H = 1/20$ on the left and the errors for $H = 1/40$ on the right. One can see that the errors of the multiscale solutions for all α cases are minor. Moreover, we observe the error reduction with a decrease in the coarse grid size.

4.1.2 Case 2: Mixed time derivatives

Let us now consider the case with mixed time-fractional derivative orders. In our numerical experiments, we set $\alpha_1 = 1.1$ and $\alpha_2 = 1.9$. Therefore, the solution field propagation is closer to the diffusion process in Ω_1 (low-conductive subregion) and closer to the wave process in Ω_2 (high-conductive subregion). In each continuum's equation of the resulting multicontinuum model, there is a linear combination of all the time derivatives. Figure 6 presents distributions of the fine-grid solution field at different time steps. Again, we see the influence of the heterogeneous structure of the diffusion coefficient on the solution. However, the obtained distributions are more concentrated and less diffused due to the mixed time-fractional derivative orders.

Figures 7 and 8 present distributions of average solutions $H = 1/40$ in Ω_1 and Ω_2 , respectively. In both figures, we depict the distributions of the reference and multiscale solutions from top to bottom. The obtained results are very similar, indicating the high accuracy of the proposed multicontinuum model.

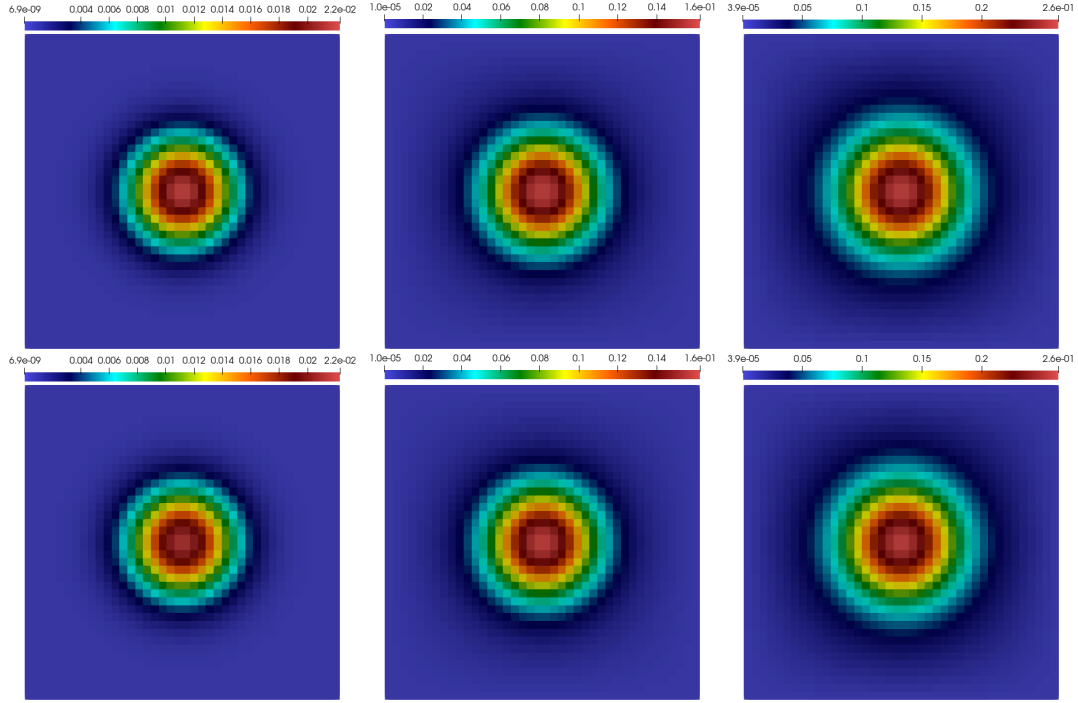


Figure 4: Average solution with $\alpha = 1.5$ at $t = 0.1, 0.5, 1$ for Case 1 in Example 1 (from left to right), $H = 1/40$. First row: reference averaged solution in Ω_1 . Second row: multiscale solution in Ω_1 .

Table 1: Relative errors at different time steps with $\alpha = 1.1$ for Case 1 in Example 1. Left: $H = 1/20$ and $l = 6$. Right: $H = 1/40$ and $l = 8$.

t	$e^{(1)}(t)$	$e^{(2)}(t)$	t	$e^{(1)}(t)$	$e^{(2)}(t)$
0.1	4.3610%	1.6115%	0.1	2.6539%	0.9813%
0.2	3.0644%	1.8407%	0.2	1.3138%	0.7866%
0.3	2.5377%	1.6898%	0.3	0.7241%	0.6480%
0.4	2.4026%	1.5983%	0.4	0.5579%	0.5979%
0.5	2.4039%	1.5183%	0.5	0.5510%	0.5295%
0.6	2.4435%	1.4562%	0.6	0.5932%	0.4655%
0.7	2.4864%	1.4169%	0.7	0.6445%	0.4228 %
0.8	2.5212%	1.3965%	0.8	0.6907%	0.3999%
0.9	2.5457%	1.3891%	0.9	0.7275%	0.3899%
1.0	2.5610%	1.3895%	1.0	0.7547%	0.3875%

Next, let us consider the errors of the multiscale solutions. Table 4 presents the relative L^2 errors at different time steps for $\alpha_1 = 1.1$ and $\alpha_2 = 1.9$. From left to right, we depict the errors for the coarse grid sizes $H = 1/20$ and $H = 1/40$. One can see that the errors are small for both continua and coarse-grid sizes. We observe the errors decreasing with the decreasing of the coarse-grid size H , as expected.

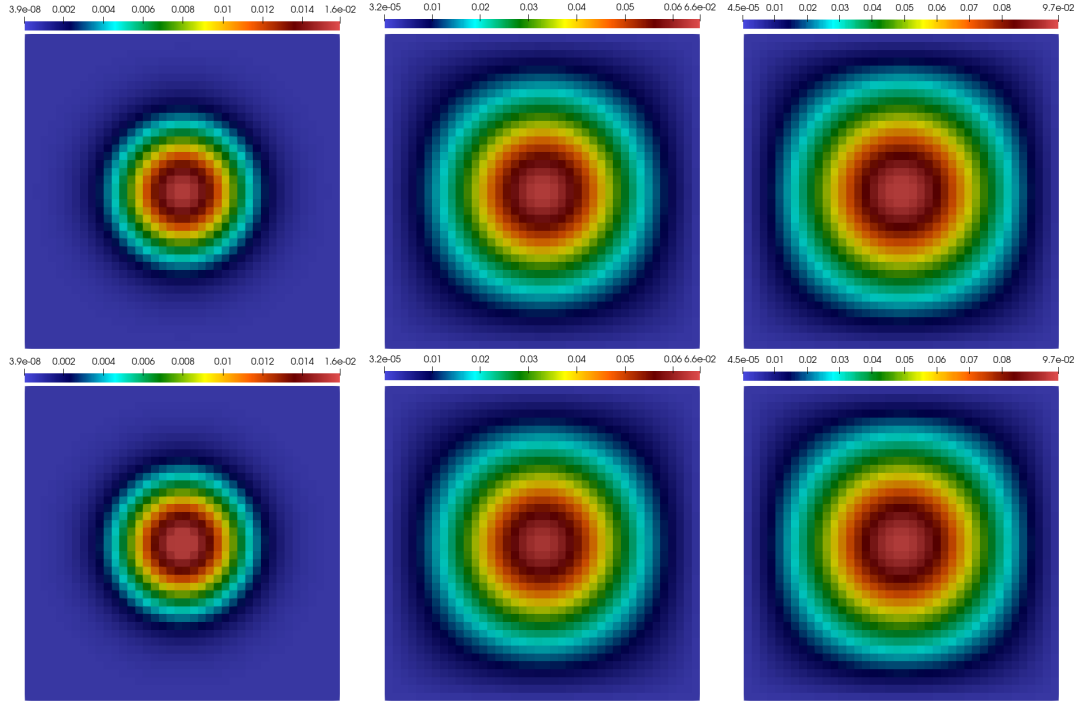


Figure 5: Average solution with $\alpha = 1.5$ at $t = 0.1, 0.5, 1$ for Case 1 in Example 1 (from left to right), $H = 1/40$. First row: reference averaged solution in Ω_2 . Second row: multiscale solution in Ω_2 .

Table 2: Relative errors at different time steps with $\alpha = 1.5$ for Case 1 in Example 1. Left: $H = 1/20$ and $l = 6$. Right: $H = 1/40$ and $l = 8$.

t	$e^{(1)}(t)$	$e^{(2)}(t)$	t	$e^{(1)}(t)$	$e^{(2)}(t)$
0.1	4.6637%	1.0388%	0.1	2.8759%	2.2597%
0.2	5.0996%	1.5235%	0.2	3.3907%	1.8471%
0.3	4.2770%	2.2505%	0.3	2.6049%	1.3953%
0.4	3.2231%	2.6408%	0.4	1.5417%	1.7346%
0.5	2.4167%	2.2978%	0.5	0.6943%	1.4025%
0.6	1.9937%	1.9367%	0.6	0.3017%	1.0359%
0.7	1.8844%	1.8525%	0.7	0.3072%	1.0668%
0.8	1.9575%	1.7751%	0.8	0.3176%	1.0312%
0.9	2.1136%	1.6038%	0.9	0.3493%	0.8011%
1.0	2.2911%	1.4076%	1.0	0.4593%	0.5027%

Table 3: Relative errors at different time steps with $\alpha = 1.9$ for Case 1 in Example 1. Left: $H = 1/20$ and $l = 6$. Right: $H = 1/40$ and $l = 8$.

t	$e^{(1)}(t)$	$e^{(2)}(t)$	t	$e^{(1)}(t)$	$e^{(2)}(t)$
0.1	3.2835%	1.2876%	0.1	1.4581%	0.7435%
0.2	4.5091%	0.9312%	0.2	2.7035%	2.3210%
0.3	5.3425%	1.6117%	0.3	3.5888%	2.8675%
0.4	5.4649%	1.8804%	0.4	3.7700%	2.4045%
0.5	4.9539%	2.5350%	0.5	3.3087%	2.0839%
0.6	4.0613%	3.5565%	0.6	2.4581%	2.7680%
0.7	3.0423%	4.2390%	0.7	1.4846%	3.5367%
0.8	2.1076%	4.0676%	0.8	0.6802%	3.4962%
0.9	1.4487%	3.1557%	0.9	0.7163%	2.5995%
1.0	1.1994%	2.5295%	1.0	1.1724%	1.9349%

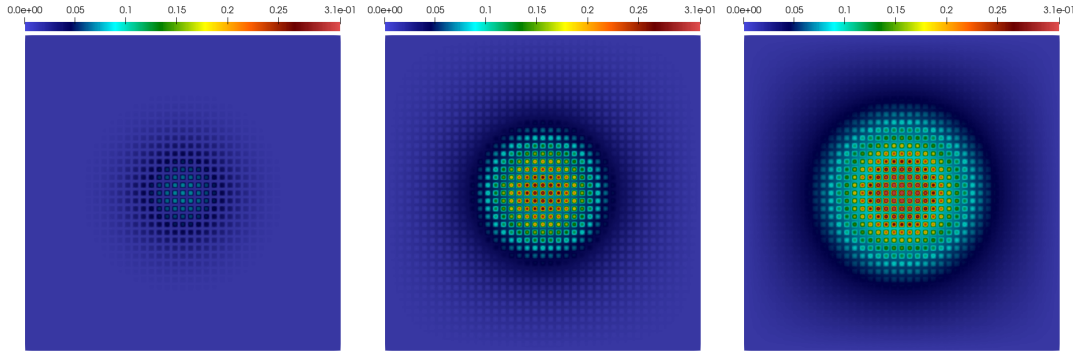


Figure 6: The fine-grid reference solution with $\alpha_1 = 1.1$, $\alpha_2 = 1.9$ at $t = 0.1, 0.5, 1$ for Case 2 in Example 1 (from left to right).

Table 4: Relative errors at different time steps with $\alpha_1 = 1.1, \alpha_2 = 1.9$ for Case 2 in Example 1. Left: $H = 1/20$ and $l = 6$. Right: $H = 1/40$ and $l = 8$.

t	$e^{(1)}(t)$	$e^{(2)}(t)$	t	$e^{(1)}(t)$	$e^{(2)}(t)$
0.1	5.0774%	3.0555%	0.1	3.4044%	3.4382%
0.2	3.0151%	2.5509%	0.2	0.9572%	0.9120%
0.3	2.8921%	2.6385%	0.3	0.8672%	0.9831%
0.4	2.8242%	2.2639%	0.4	0.7755%	0.8696%
0.5	2.6937%	1.8062%	0.5	0.7030%	0.6527%
0.6	2.5482%	1.4270%	0.6	0.6655%	0.4656%
0.7	2.4243%	1.1835%	0.7	0.6574%	0.3468%
0.8	2.3341%	1.0884%	0.8	0.6573%	0.2877%
0.9	2.2852%	1.1084%	0.9	0.6604%	0.2733%
1.0	2.2825%	1.2035%	1.0	0.6756%	0.2944%

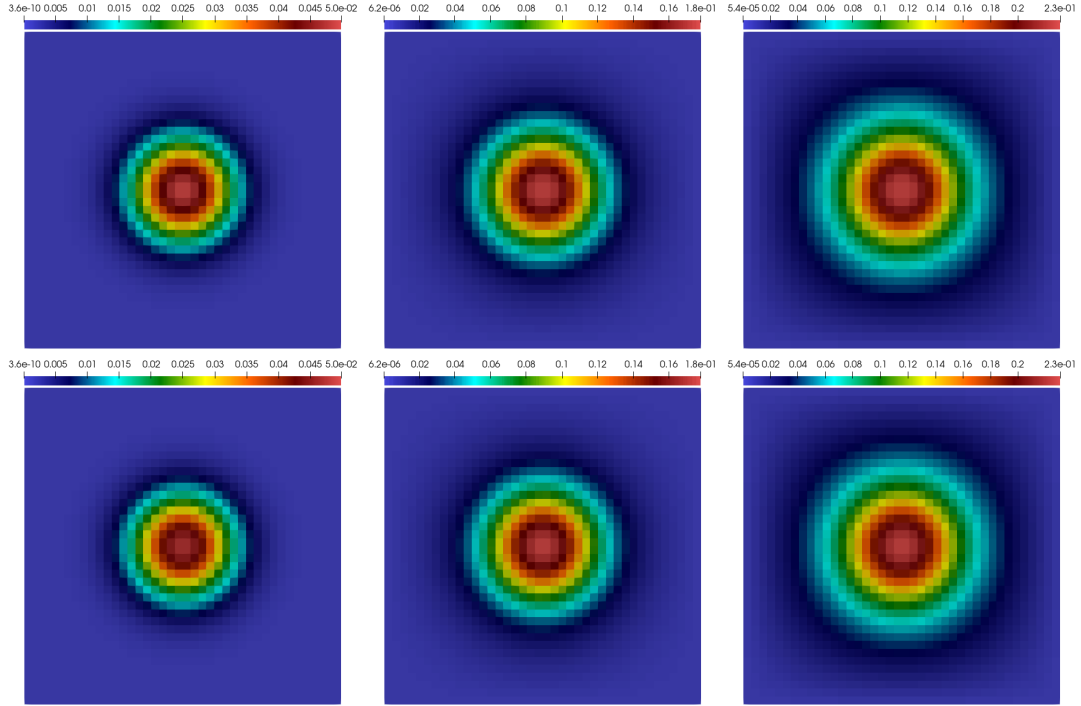


Figure 7: Average solution with $\alpha_1 = 1.1$, $\alpha_2 = 1.9$ at $t = 0.1, 0.5, 1$ for Case 2 in Example 1 (from left to right), $H = 1/40$. First row: reference averaged solution in Ω_1 . Second row: multiscale solution in Ω_1 .

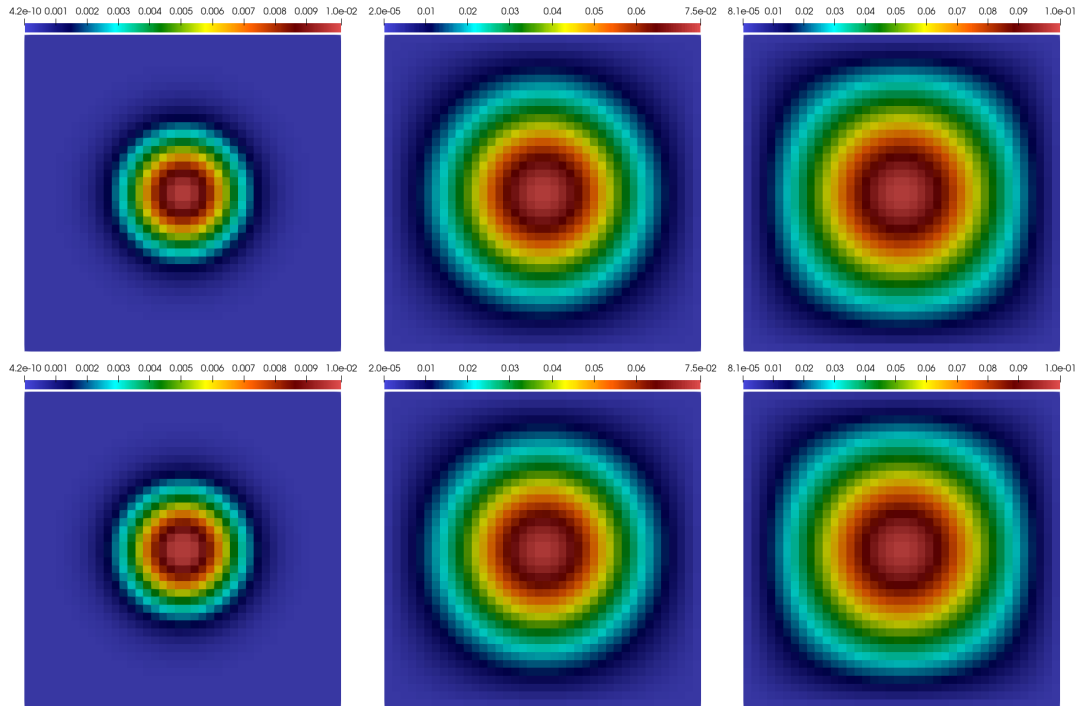


Figure 8: Average solution with $\alpha_1 = 1.1$, $\alpha_2 = 1.9$ at $t = 0.1, 0.5, 1$ for Case 2 in Example 1 (from left to right), $H = 1/40$. First row: reference averaged solution in Ω_2 . Second row: multiscale solution in Ω_2 .

4.2 Example 2: Layered field

As in the previous example, we define κ using (41), but we consider a layered structure depicted in Figure 9. The source term f is given as $f(x) = e^{-40((x_1-0.5)^2+(x_2-0.5)^2)}$ for any $x = (x_1, x_2) \in \Omega$. Also, we set the initial condition $u_0 = u(x, 0) = 0.5e^{-40((x_1-0.5)^2+(x_2-0.5)^2)}$ and impose zero Neumann boundary condition

$$\frac{\partial u}{\partial n} = 0, \quad x \in \partial\Omega. \quad (43)$$

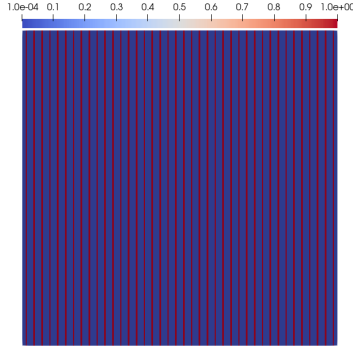


Figure 9: The coefficient κ (Ω_1 : blue regions; Ω_2 : red regions). Layered field.

Again, we consider both regular and mixed cases of time-fractional derivative orders in the following numerical experiments.

4.2.1 Case 1: Regular time derivatives

In this case, we set the time fractional order derivative $\alpha = 1.2$ for both continua. Figure 10 depicts distributions of the fine-grid solution field at different time steps. One can see the influence of the layered structure of the heterogeneous diffusion coefficient. The initial distribution of the solution gradually propagates along the vertical directions due to the high conductivity of the channels. The obtained numerical results correspond to the simulated process.

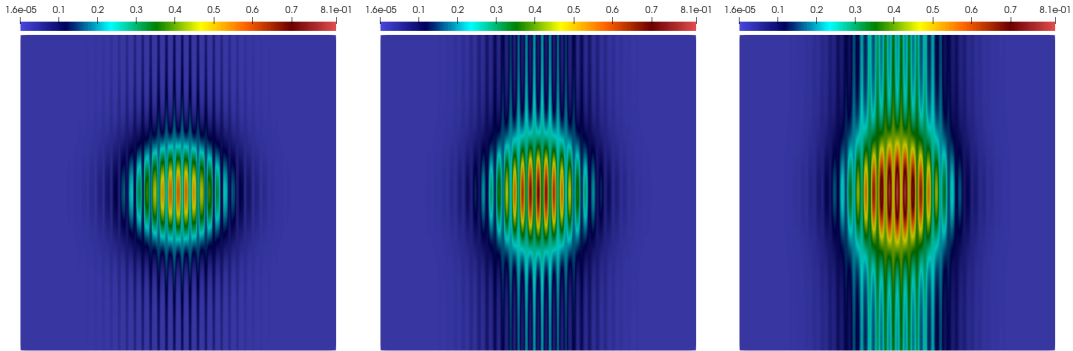


Figure 10: The fine-grid reference solution with $\alpha = 1.2$ at $t = 0.1, 0.5, 1$ for Case 1 in Example 2 (from left to right).

Next, let us consider the average solutions of the reference and multiscale solutions. In Figures 11 and 12, we present distributions of the average solutions in Ω_1 and Ω_2 with $H = 1/40$, respectively. From top to bottom, we depict the reference and multiscale solutions. As in the previous example, we see that the obtained results are very similar. Moreover, one can notice that the solution propagation has an

anisotropic nature due to the structure of the high-contrast diffusion coefficient. We observe more rapid propagation of the average solution in Ω_2 than in Ω_1 , as expected.

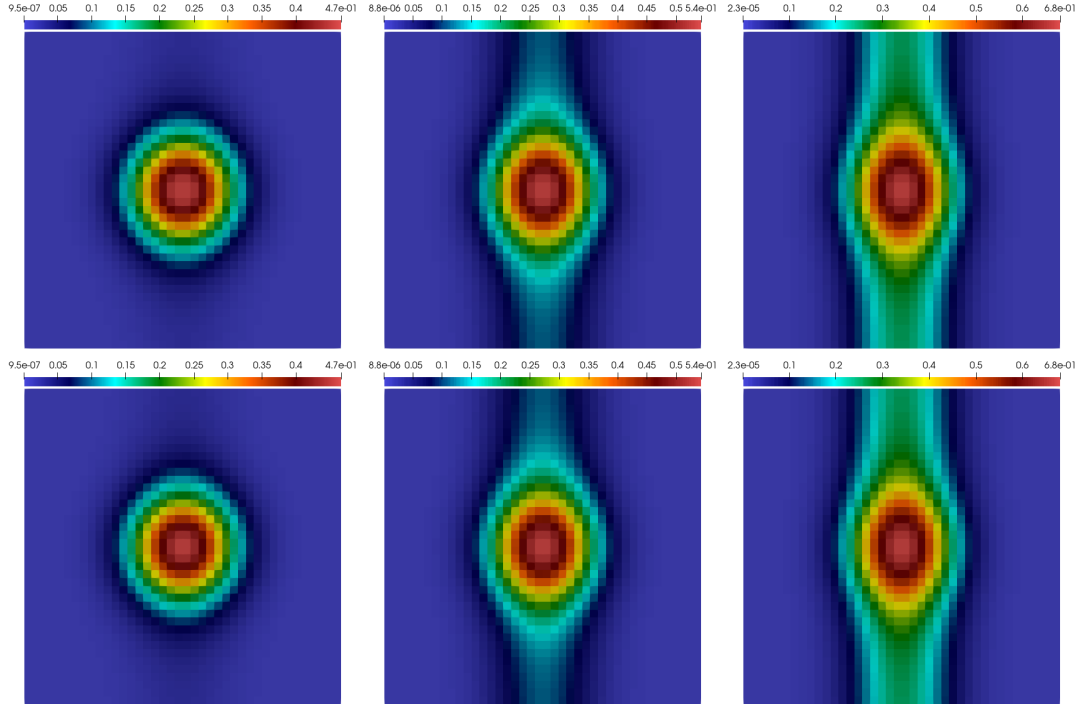


Figure 11: Average solution with $\alpha = 1.2$ at $t = 0.1, 0.5, 1$ for Case 1 in Example 2 (from left to right), $H = 1/40$. First row: reference averaged solution in Ω_1 . Second row: multiscale solution in Ω_1 .

Let us consider the errors of the multiscale solution. In Table 5, we present the relative L^2 errors of the average multiscale solutions at different time steps. From left to right, we have the errors for coarse-grid sizes $H = 1/20$ and $H = 1/40$. One can see that the errors are minor for both coarse grids. One can see that the errors gradually decrease with time. Moreover, the smaller the coarse-grid size, the higher the accuracy we achieve. Therefore, our multicontinuum approach can approximate the reference solution with high accuracy.

Table 5: Relative errors at different time steps with $\alpha = 1.2$ for Case 1 in Example 2. Left: $H = 1/20$ and $l = 6$. Right: $H = 1/40$ and $l = 8$.

t	$e^{(1)}(t)$	$e^{(2)}(t)$	t	$e^{(1)}(t)$	$e^{(2)}(t)$
0.1	3.4643%	3.0195%	0.1	1.7997%	1.9799%
0.2	2.3059%	3.7543%	0.2	0.5696%	2.8582%
0.3	2.0710%	1.9225%	0.3	0.4282%	0.8036%
0.4	2.1109%	1.5818%	0.4	0.4650%	0.4468%
0.5	2.1660%	1.5747%	0.5	0.5128%	0.4341%
0.6	2.1843%	1.5947%	0.6	0.5614%	0.4056%
0.7	2.1728%	1.5984%	0.7	0.5940%	0.4081%
0.8	2.1416%	1.5965%	0.8	0.6084%	0.4162%
0.9	2.1021%	1.5849%	0.9	0.6124%	0.4143%
1.0	2.0577%	1.5777%	1.0	0.6078%	0.4154%

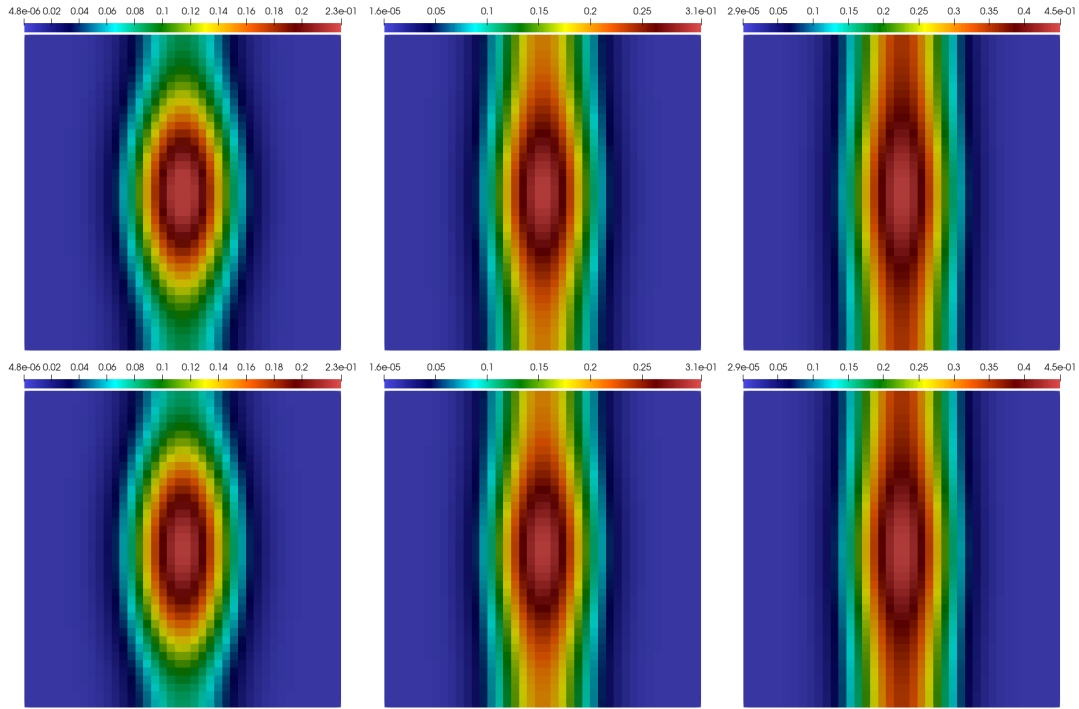


Figure 12: Average solution with $\alpha = 1.2$ at $t = 0.1, 0.5, 1$ for Case 1 in Example 2 (from left to right), $H = 1/40$. First row: reference averaged solution in Ω_2 . Second row: multiscale solution U_2 in Ω_2 .

4.2.2 Case 2: Mixed time derivatives

Finally, let us consider the case with mixed time-fractional derivative orders. Again, we set $\alpha_1 = 1.1$ in Ω_1 and $\alpha_2 = 1.9$ in Ω_2 . Therefore, the solution propagation in the high-conductive channels is closer to the wave process, while the spread in the low-conductive subregions is closer to the diffusion process. Figure 13 shows distributions of the fine-grid solution at different time steps. One can see the changes in the solution distributions compared to the previous case due to the mixed time-fractional derivatives. It is especially noticeable in the high-conductive channels at the time instant $t = 0.4$.

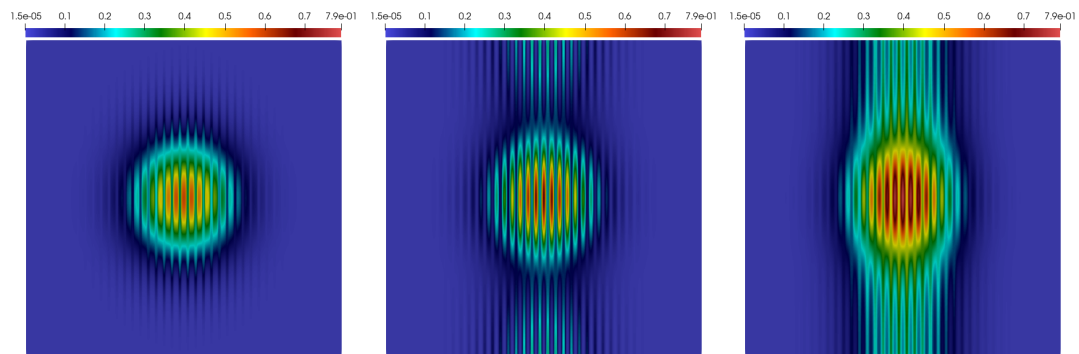


Figure 13: The fine-grid reference solution with $\alpha_1 = 1.1$, $\alpha_2 = 1.9$ at $t = 0.1, 0.4, 1$ for Case 2 in Example 2 (from left to right).

Figures 14 and 15 present distributions of the average solution fields with $H = 1/40$ in Ω_1 and Ω_2 , respectively. We depict the reference average solution on the top and the multiscale solution on the

bottom. One can see that our multiscale solutions are very similar to the reference ones, indicating high accuracy. Compared to the previous case, the average solution in Ω_1 changed regarding ranges but mostly remained the dynamics. In contrast, we can see the changes in the dynamics of the average solution in Ω_2 due to the mixed time-fractional derivatives. The differences are more noticeable at the time instants $t = 0.1$ and $t = 0.4$.

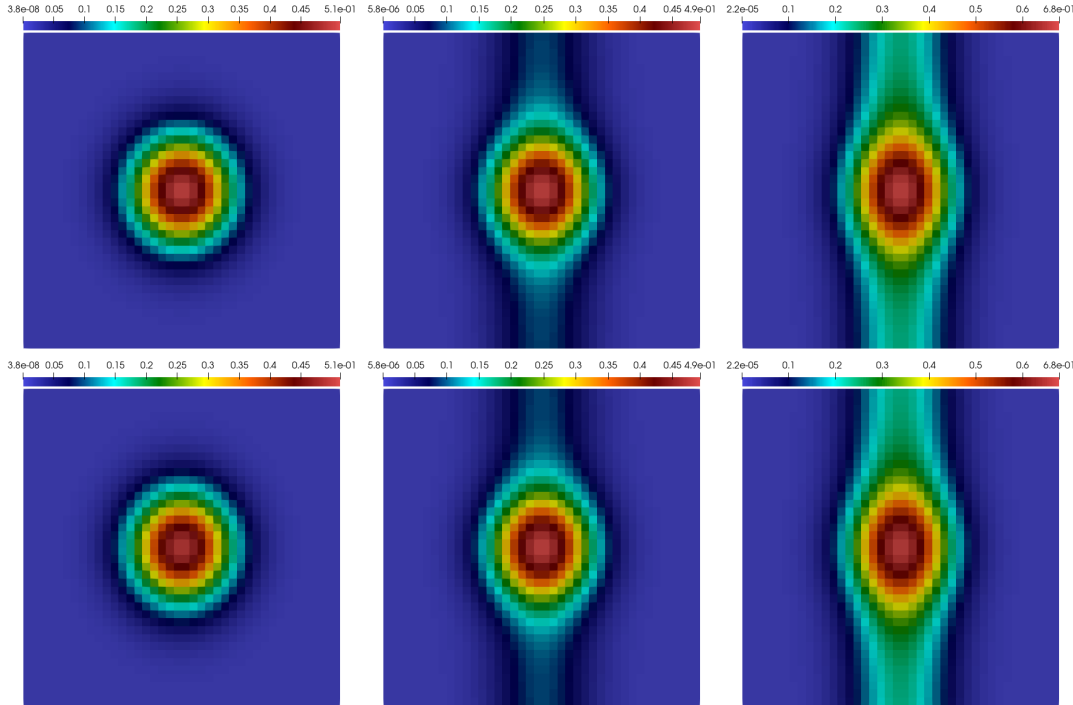


Figure 14: Average solution with $\alpha_1 = 1.1$, $\alpha_2 = 1.9$ at $t = 0.1, 0.4, 1$ for Case 2 in Example 2 (from left to right), $H = 1/40$. First row: reference averaged solution in Ω_1 . Second row: multiscale solution in Ω_1 .

Next, let us consider the errors of our multicontinuum approach. Table 6 presents the relative L^2 errors at different time steps for both continua using $H = 1/20$ and $H = 1/40$. One can see that all the errors are minor. We can observe the reduction in the errors with a decrease in the coarse-grid size H .

Table 6: Relative errors at different time steps with $\alpha_1 = 1.1, \alpha_2 = 1.9$ for Case 2 in Example 2. Left: $H = 1/20$ and $l = 6$. Right: $H = 1/40$ and $l = 8$.

t	$e^{(1)}(t)$	$e^{(2)}(t)$	t	$e^{(1)}(t)$	$e^{(2)}(t)$
0.1	3.6809%	2.6249%	0.1	1.8825%	0.6262%
0.2	2.9735%	2.8666%	0.2	1.1861%	0.7398%
0.3	2.3455%	2.8279%	0.3	0.7846%	0.7883%
0.4	2.1554%	2.1954%	0.4	0.5348%	0.9551%
0.5	2.3374%	2.2074%	0.5	0.7289%	1.2642%
0.6	2.2823%	1.8027%	0.6	0.6791%	0.9199%
0.7	2.0348%	1.6265%	0.7	0.5695%	0.5843%
0.8	2.0175%	1.5654%	0.8	0.6366%	0.6088%
0.9	2.1512%	1.7002%	0.9	0.7034%	0.7133%
1.0	2.1917%	1.7845%	1.0	0.6888%	0.5972%

Therefore, our multicontinuum approach can provide high accuracy for different types of hetero-

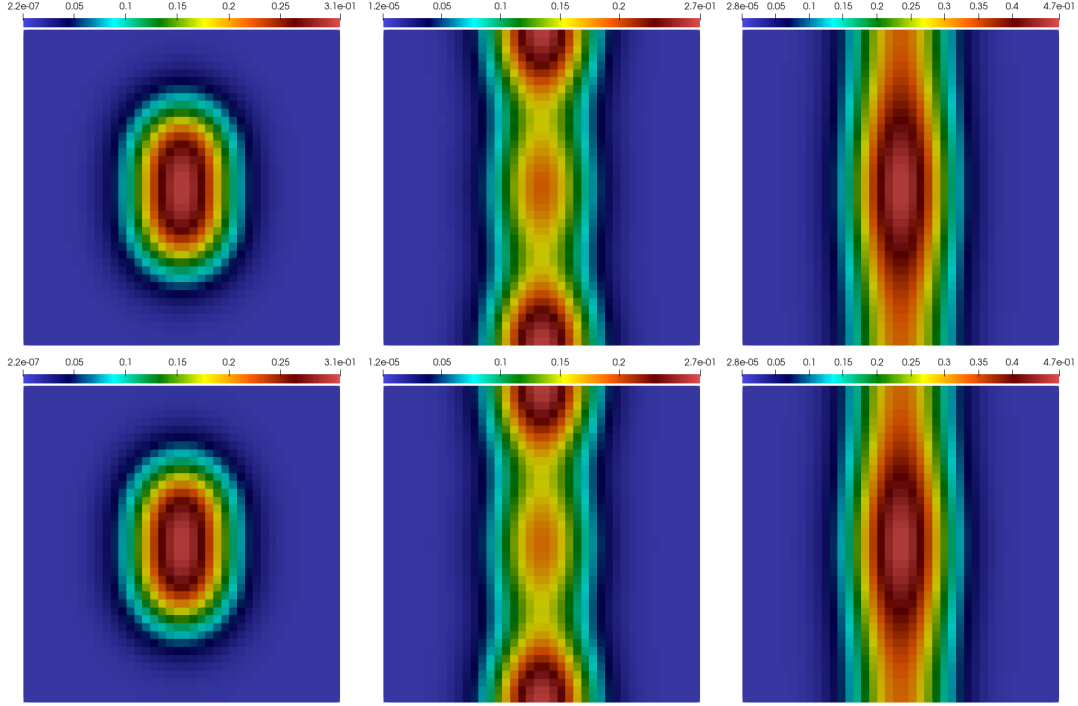


Figure 15: Average solution with $\alpha_1 = 1.1$, $\alpha_2 = 1.9$ at $t = 0.1, 0.4, 1$ for Case 2 in Example 2 (from left to right), $H = 1/40$. First row: reference averaged solution in Ω_2 . Second row: multiscale solution in Ω_2 .

genities that can result in isotropic and anisotropic propagation. Moreover, it can accurately capture different time-fractional derivative orders, including the case with different orders in different continua.

5 Conclusion

In this work, we have applied the multicontinuum homogenization method to derive the multicontinuum time-fractional diffusion-wave model. First, we formulated constraint cell problems in oversampled regions considering gradient effects and averages. By solving the constraint cell problems, we obtained multicontinuum expansions of the fine-scale solution. Then, we rigorously derived the multicontinuum models for two cases of time-fractional derivatives. In the first case, time-fractional orders are the same for all continua. The second case represents the mixed time-fractional derivatives, where we have different orders in different continua. To check the effectiveness of the proposed multicontinuum approach, we have conducted numerical experiments by solving model problems with two continua. The results show that our multicontinuum models can provide high accuracy for different heterogeneous media and time-fractional derivatives.

Acknowledgments

The research of Huiran Bai is supported by the Postgraduate Scientific Research Innovation Project of Xiangan University (XDCX2024Y160) and the Chinese Government Scholarship (CSC No. 202408430165).

The research of Yin Yang and Wei Xie is supported by the National Natural Science Foundation of China Project (No. 12261131501), National Foreign Experts Program (No.S20240066), the Project of Scientific Research Fund of the Hunan Provincial Science and Technology Department (No.2023GK2029, No.2024JC1003, No.2024JJ1008), and “Algorithmic Research on Mathematical Common Fundamentals”

Program for Science and Technology Innovative Research Team in Higher Educational Institutions of Hunan Province of China.

The research of Dmitry Ammosov is supported by the Khalifa University Postdoctoral Fellowship Program.

References

- [1] Rumeng Zheng, Fawang Liu, and Xiaoyun Jiang. A legendre spectral method on graded meshes for the two-dimensional multi-term time-fractional diffusion equation with non-smooth solutions. *Applied Mathematics Letters*, 104:106247, 2020.
- [2] Hong Sun, Zhi-Zhong Sun, and Guang-Hua Gao. Some temporal second order difference schemes for fractional wave equations. *Numerical Methods for Partial Differential Equations*, 32(3):970–1001, 2016.
- [3] Francesco Mainardi. *Fractional calculus: some basic problems in continuum and statistical mechanics*. Springer, 1997.
- [4] Ralf Metzler and Joseph Klafter. The random walk’s guide to anomalous diffusion: a fractional dynamics approach. *Physics reports*, 339(1):1–77, 2000.
- [5] VV Gafiychuk and B Yo Datsko. Pattern formation in a fractional reaction–diffusion system. *Physica A: Statistical Mechanics and its Applications*, 365(2):300–306, 2006.
- [6] Rudolf Hilfer. *Applications of fractional calculus in physics*. World scientific, 2000.
- [7] Ralf Metzler and Joseph Klafter. The restaurant at the end of the random walk: recent developments in the description of anomalous transport by fractional dynamics. *Journal of Physics A: Mathematical and General*, 37(31):R161, 2004.
- [8] RR Nigmatullin. To the theoretical explanation of the “universal response”. *physica status solidi (b)*, 123(2):739–745, 1984.
- [9] RR Nigmatullin. The realization of the generalized transfer equation in a medium with fractal geometry. *Physica status solidi (b)*, 133(1):425–430, 1986.
- [10] Francesco Mainardi and Paolo Paradisi. Fractional diffusive waves. *Journal of Computational Acoustics*, 9(04):1417–1436, 2001.
- [11] Zhi-zhong Sun and Xiaonan Wu. A fully discrete difference scheme for a diffusion-wave system. *Applied Numerical Mathematics*, 56(2):193–209, 2006.
- [12] Rui Du, WR Cao, and ZZ Sun. A compact difference scheme for the fractional diffusion-wave equation. *Applied Mathematical Modelling*, 34(10):2998–3007, 2010.
- [13] Ya-Nan Zhang, Zhi-zhong Sun, and Xuan Zhao. Compact alternating direction implicit scheme for the two-dimensional fractional diffusion-wave equation. *SIAM Journal on Numerical Analysis*, 50(3):1535–1555, 2012.
- [14] Xiaolin Li and Shuling Li. A fast element-free galerkin method for the fractional diffusion-wave equation. *Applied Mathematics Letters*, 122:107529, 2021.
- [15] Anatoly A Alikhanov, Mohammad Shahbazi Asl, Chengming Huang, and Aslanbek Khibiev. A second-order difference scheme for the nonlinear time-fractional diffusion-wave equation with generalized memory kernel in the presence of time delay. *Journal of Computational and Applied Mathematics*, 438:11515, 2024.

- [16] Donald L Brown and Maria Vasilyeva. A generalized multiscale finite element method for poroelasticity problems i: Linear problems. *Journal of Computational and Applied Mathematics*, 294:372–388, 2016.
- [17] Barrett Baldwin and Timothy Barth. A one-equation turbulence transport model for high reynolds number wall-bounded flows. In *29th aerospace sciences meeting*, page 610, 1991.
- [18] Xiao-Hui Wu, Yalchin Efendiev, and Thomas Y Hou. Analysis of upscaling absolute permeability. *Discrete and Continuous Dynamical Systems Series B*, 2(2):185–204, 2002.
- [19] Ulrich Hornung. *Homogenization and porous media*, volume 6. Springer Science & Business Media, 2012.
- [20] LI Rubińštem. On a question about the propagation of heat in heterogeneous media.(russian) izvestiya akad. *Nauk SSSR. Ser. Geograf. Geofiz.*, 12:27–45, 1948.
- [21] Grigory I Barenblatt, Iu P Zheltov, and IN Kochina. Basic concepts in the theory of seepage of homogeneous liquids in fissured rocks [strata]. *Journal of applied mathematics and mechanics*, 24(5):1286–1303, 1960.
- [22] Todd Arbogast, Jim Douglas, Jr, and Ulrich Hornung. Derivation of the double porosity model of single phase flow via homogenization theory. *SIAM Journal on Mathematical Analysis*, 21(4):823–836, 1990.
- [23] GP Panasenko. Multicontinuum wave propagation in a laminated beam with contrasting stiffness and density of layers. *Journal of Mathematical Sciences*, 232:503–515, 2018.
- [24] Yalchin Efendiev and Wing Tat Leung. Multicontinuum homogenization and its relation to nonlocal multicontinuum theories. *Journal of Computational Physics*, 474:111761, 2023.
- [25] E Chung, Yalchin Efendiev, Juan Galvis, and Wing Tat Leung. Multicontinuum homogenization. general theory and applications. *Journal of Computational Physics*, 510:112980, 2024.
- [26] Wing Tat Leung. Some convergence analysis for multicontinuum homogenization. *arXiv preprint arXiv:2401.12799*, 2024.
- [27] Wei Xie, Yalchin Efendiev, Yunqing Huang, Wing Tat Leung, and Yin Yang. Multicontinuum homogenization in perforated domains. *arXiv preprint arXiv:2404.17471*, 2024.
- [28] Dmitry Ammosov, WT Leung, Buzheng Shan, and Jian Huang. Multicontinuum homogenization for coupled flow and transport equations. *arXiv preprint arXiv:2405.14572*, 2024.
- [29] Dmitry Ammosov, Sergei Stepanov, Denis Spiridonov, and Wenyuan Li. Multicontinuum homogenization for richards’ equation: The derivation and numerical experiments. *Russian Journal of Numerical Analysis and Mathematical Modelling*, 38(4):207–218, 2023.
- [30] Yalchin Efendiev, Wing Tat Leung, Buzheng Shan, and Min Wang. Multicontinuum splitting scheme for multiscale flow problems. *arXiv preprint arXiv:2410.05253*, 2024.
- [31] Patrick Jenny, SH Lee, and Hamdi A Tchelepi. Multi-scale finite-volume method for elliptic problems in subsurface flow simulation. *Journal of computational physics*, 187(1):47–67, 2003.
- [32] Ivan Lunati and Patrick Jenny. Multiscale finite-volume method for compressible multiphase flow in porous media. *Journal of Computational Physics*, 216(2):616–636, 2006.
- [33] Omar Chaabi and Mohammed Al Kobaisi. Algorithmic monotone multiscale finite volume methods for porous media flow. *Journal of Computational Physics*, 499:112739, 2024.

- [34] Thomas Y Hou and Xiao-Hui Wu. A multiscale finite element method for elliptic problems in composite materials and porous media. *Journal of computational physics*, 134(1):169–189, 1997.
- [35] Thomas Hou, Xiao-Hui Wu, and Zhiqiang Cai. Convergence of a multiscale finite element method for elliptic problems with rapidly oscillating coefficients. *Mathematics of computation*, 68(227):913–943, 1999.
- [36] Yalchin Efendiev and Thomas Y Hou. *Multiscale finite element methods: theory and applications*, volume 4. Springer Science & Business Media, 2009.
- [37] Shan Jiang, Meiling Sun, and Yin Yang. Reduced multiscale computation on adapted grid for the convection-diffusion robin problem. *Journal of Applied Analysis and Computation*, 7(4):1488–1502, 2017.
- [38] Yalchin Efendiev, Juan Galvis, and Thomas Y Hou. Generalized multiscale finite element methods (gmsfem). *Journal of computational physics*, 251:116–135, 2013.
- [39] Eric T Chung, Yalchin Efendiev, and Wing Tat Leung. Generalized multiscale finite element methods for wave propagation in heterogeneous media. *Multiscale Modeling & Simulation*, 12(4):1691–1721, 2014.
- [40] Eric T Chung, Yalchin Efendiev, and Shubin Fu. Generalized multiscale finite element method for elasticity equations. *GEM-International Journal on Geomathematics*, 5:225–254, 2014.
- [41] Eric Chung, Yalchin Efendiev, and Thomas Y Hou. Adaptive multiscale model reduction with generalized multiscale finite element methods. *Journal of Computational Physics*, 320:69–95, 2016.
- [42] Wei Xie, Juan Galvis, Yin Yang, and Yunqing Huang. On time integrators for generalized multiscale finite element methods applied to advection–diffusion in high-contrast multiscale media. *Journal of Computational and Applied Mathematics*, 460:116363, 2025.
- [43] Eric T Chung, Yalchin Efendiev, and Wing Tat Leung. Constraint energy minimizing generalized multiscale finite element method. *Computer Methods in Applied Mechanics and Engineering*, 339:298–319, 2018.
- [44] Eric Chung, Jiuhua Hu, and Sai-Mang Pun. Convergence of the cem-gmsfem for stokes flows in heterogeneous perforated domains. *Journal of Computational and Applied Mathematics*, 389:113327, 2021.
- [45] Wei Xie, Yin Yang, Eric Chung, and Yunqing Huang. Cem-gmsfem for poisson equations in heterogeneous perforated domains. *Multiscale Modeling & Simulation*, 22(4):1683–1708, 2024.
- [46] Aleksei Tyrylgin, Maria Vasilyeva, Anatoly Alikhanov, and Dongwoo Sheen. A computational macroscale model for the time fractional poroelasticity problem in fractured and heterogeneous media. *Journal of Computational and Applied Mathematics*, 418:114670, 2023.
- [47] Wenyuan Li, Anatoly Alikhanov, Yalchin Efendiev, and Wing Tat Leung. Partially explicit time discretization for nonlinear time fractional diffusion equations. *Communications in Nonlinear Science and Numerical Simulation*, 113:106440, 2022.
- [48] Anatoly Alikhanov, Huiran Bai, Jian Huang, Aleksei Tyrylgin, and Yin Yang. Multiscale model reduction for the time fractional thermoporoelasticity problem in fractured and heterogeneous media. *Journal of Computational and Applied Mathematics*, 455:116157, 2025.
- [49] Anders Logg, Kent-Andre Mardal, and Garth Wells. *Automated solution of differential equations by the finite element method: The FEniCS book*, volume 84. Springer Science & Business Media, 2012.
- [50] James Ahrens, Berk Geveci, and Charles Law. Paraview: An end-user tool for large data visualization. *The visualization handbook*, 717, 2005.